

Magnetism and Charge Dynamics in Iron Pnictides

Z. P. Yin, K. Haule, and G. Kotliar

Department of Physics and Astronomy, Rutgers University, Piscataway, NJ 08854, United States.

(Dated: July 20, 2010)

In a wide variety of materials, such as layered copper oxides, heavy fermions, organic salts, and the recently discovered iron pnictides, superconductivity is found in close proximity to a magnetically ordered state^{1,2}. The character of the proximate magnetic phase is thus believed to be crucial for understanding the differences between the various families of unconventional superconductors and the mechanism of superconductivity. Unlike the antiferromagnetic order in cuprates, which is well described by the spin Heisenberg model, the nature of the magnetism and of the underlying electronic state in the iron pnictide superconductors is not well understood. Neither density functional theory nor models based on atomic physics and superexchange, account for the small size of the magnetic moment³. Many low energy probes such as transport⁴, scanning tunneling microscopy⁵ and angle-resolved photoemission spectroscopy (ARPES)[6] measured strong anisotropy of the electronic states akin to the nematic order in a liquid crystal, but there is no consensus on its physical origin, and a three dimensional picture of electronic states and its relations to the optical conductivity in the magnetic state is lacking. Using a first principles approach, we obtained the experimentally observed magnetic moment, optical conductivity, and the anisotropy of the electronic states. The theory connects ARPES, which measures one particle electronic states, optical spectroscopy, probing the particle hole excitations of the solid and neutron scattering which measures the magnetic moment. We predict a manifestation of the anisotropy in the optical conductivity, and we show that the magnetic phase arises from the paramagnetic phase by a large gain of the Hund's rule coupling energy and a smaller loss of kinetic energy, indicating that iron pnictides represent a new class of compounds where the nature of magnetism is intermediate between the spin density wave of almost independent particles, and the antiferromagnetic state of local moments.

Below the Neel temperature of the order of 150 K the parent compounds of the iron pnictide superconductors remain metallic with a magnetization density oscillating in space (spin density wave, SDW). The sublattice magnetization is concentrated on iron atoms and its arrangement in space is antiferromagnetic in the x direction and ferromagnetic in the y direction⁷.

We use the combination of the density functional the-

ory (DFT) with local density approximation (LDA) and the dynamical mean field theory (DMFT)[8] to study the archetypical iron pnictide compound BaFe_2As_2 in both the magnetic SDW and the paramagnetic (PM) state. The size of the theoretical magnetic moment is $0.86 \mu_B$, similar to the measured moment of $0.87 \mu_B$ [3], but much smaller than $1.75 \mu_B$ [9] obtained by the local spin density approximation (LSDA) within DFT. The considerably smaller magnetic moment obtained here is due to the fact that the competing PM metallic state is a correlated metal, which contains very fast fluctuating moments in time, but no static moment. Only a small part of these fluctuating moments acquires a static component in the ordered state.

The onset of magnetic order has a profound impact on the electronic structure, and these changes are probed by optical spectroscopy. Figure 1(a) shows the in-plane (averaged over x and y direction) optical conductivity of BaFe_2As_2 in the SDW and PM states calculated by both LDA+DMFT and L(S)DA. Fig. 1(b) reproduces measured in-plane optical conductivity from Refs. 10 and 11. Both theory and experiments^{10,11} show a reduction of the low frequency Drude peak, which indicates a removal of a large fraction of carriers in the ordered state. Our calculation captures all the important qualitative features measured in experiments. In both PM and SDW states there is a broad peak due to interband transitions centered around 5500 cm^{-1} [12]. Below 2000 cm^{-1} the optical conductivity of the SDW phase shows a few extra excitations appearing as peak and shoulders centered at 1250 cm^{-1} (arrow 2 in cyan), shoulder structure at about 800 cm^{-1} (arrow 1 in blue), and a small peak at 1800 cm^{-1} (arrow 3 in green). These additional excitations appear in experiment at slightly smaller energies, as seen in Figs. 1(a) and (b).

These extra peaks and shoulders strongly depend on the polarization of the light, as shown in Fig. 1(c), where we plot separately the x and the y component of the optical conductivity. The first two excitations (blue arrow 1 and cyan arrow 2) are much more pronounced in the x direction, while the third peak (green arrow 3) is more pronounced in the y direction. Also the conductivity is considerably larger in the x direction (antiparallel spins) than in the y direction (parallel spins). At low frequency, the optical conductivity of the SDW phase shows Drude like behavior, with Drude weight considerable smaller than in the PM phase. The theoretical value of the plasma frequency for the x , y and z direction (1.14, 0.88 and 0.69 eV, respectively) are much smaller than the plasma frequency of 1.60 eV of the PM DMFT calculation¹², which agrees very well with experimental esti-

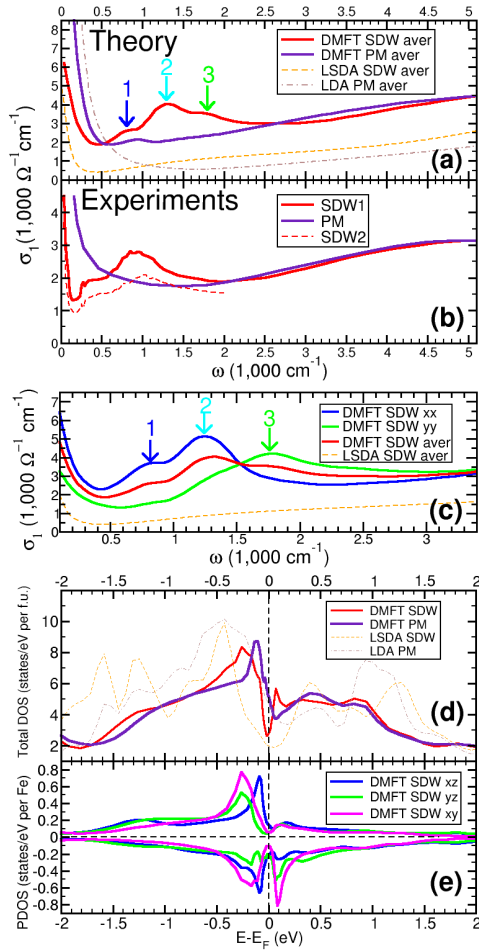


FIG. 1: Optical conductivity and DOS of BaFe₂As₂. (a)calculated in-plane average optical conductivity by LDA+DMFT and L(S)DA in the SDW and PM states; (b)experimental in-plane optical conductivity in the SDW and PM states. Data are taken from Refs.[10] and [11]; (c)the xx , yy , and in-plane average optical conductivity in the SDW state calculated by LDA+DMFT and LSDA (only the average is shown for LSDA); (d)total DOS in the SDW and PM states calculated by LDA+DMFT and L(S)DA and (e)the projected DOS of Fe 3d xz , yz and xy orbitals in the SDW state calculated by LDA+DMFT, plotting positive/negative for majority/minority spin.

mates^{10,13}. This reduction was also observed experimentally¹⁰. The anisotropy of the in-plane optical conductivity has not been studied experimentally, because of the fairly coarse spatial resolution imposed by the diffraction limit, spanning multiple magnetic domains. Near field optics¹⁴, or techniques to prepare monodomain samples⁴, are promising avenues to test our prediction.

It is useful to analyze the optical conductivity at various frequency scales. The Drude weight is controlled by the Fermi surface size, and by the mass enhancement of the low energy quasiparticles. In the SDW state, the mass enhancement is smaller (2, 1.7, 1.7 and 1.5 for the $t2g$ /majority, $t2g$ /minority, eg /majority, and

eg /minority orbitals) than in the PM state (3 and 2, for the $t2g$ and eg orbitals, respectively). While the quasiparticles become lighter in the SDW phase, the Fermi surface area is much smaller, and the latter effect dominates, resulting in a reduction of the Drude weight.

We also integrated the in-plane optical conductivity to obtain the effective kinetic energy of a low energy model, in both the SDW phase and the PM phase. At very low energies, the onset of magnetism results in an *increase* of the optical conductivity, due to the coherence-incoherence crossover. The long range order makes the material more coherent. Consequently the very low energy model gains kinetic energy in the ordered state. At intermediate energies, however, kinetic energy is lost as the result of the opening of the SDW gap on the Fermi surface.

Since the optical conductivity of the PM phase is quite temperature dependent, we compare the SDW phase and PM phase at the same temperature ($T = 72.5\text{K}$), the latter being a metastable state at low temperature. Using this procedure, we find that the missing weight from opening the SDW gap is recovered only around 10000cm^{-1} , many times larger scale than the gap value. This should be contrasted with the classic weakly correlated materials, where the spectral weight is recovered immediately above the SDW gap.

Recent dc conductivity and scanning tunneling microscopy (STM) measurements have detected a large anisotropy in the ab plane.⁴⁵ The theoretical zero frequency limit of the optical conductivity is 7350 , 4400 , and $3350 \Omega^{-1}\text{cm}^{-1}$ for the xx , yy and zz components, respectively. This implies that the resistivity in the y direction is about 1.67 times of that in the x direction, in good agreement with the results of resistivity measurements of Chu *et al.*⁴.

We now turn to electronic density of states. Figure1(d) shows the total density of states (DOS) in both the PM and SDW phases. In the SDW phase, DMFT DOS shows a clear pseudogap on the scale of 0.15eV around the Fermi level, in good agreement with STM measurements⁵. The LSDA DOS also shows a pseudogap at the Fermi level¹⁵, however, its width is more than 0.5eV , therefore LSDA misses the structure below 4000cm^{-1} in the optical conductivity.

The onset of stripe magnetic phase is also accompanied by a rearrangement of the iron crystal field states, which gives rise to orbital polarization. This polarization is uniform in space (ferro-orbital ordering), as surmised by Singh¹⁶. The partial density of states of an Fe atom is shown in Fig.1(e). The minority density is given a negative sign. To extract the anisotropy of the electronic structure, we integrate the partial density of states of xz and yz orbital ($A_{xz}(\omega)$ and $A_{yz}(\omega)$) to obtain their occupation, and evaluate their difference $\Delta n(\Lambda) = \int_{-\Lambda}^0 [A_{xz}(\omega) - A_{yz}(\omega)] d\omega / (\frac{1}{2} \int_{-\Lambda}^0 [A_{xz}(\omega) + A_{yz}(\omega)] d\omega)$. This defines the energy dependent orbital polarization. For large cutoff Λ , the orbital polarization is close to zero for majority electrons and around 0.13 for minority

electrons. At low energy, the anisotropy is enhanced to 1.23 (0.45) for majority (minority) carriers, when Λ is 0.15 eV, the size of the optical SDW gap.

The anisotropy of the partial density of states provides a natural explanation for the anisotropy in the optical conductivity; the yz density of states has less electronic states at the Fermi level and the main peak of the yz orbital is further away from the Fermi level compared to xz orbital. The optical conductivity in x direction comes primarily from xz and xy orbitals, and is thus larger than the conductivity in y direction, which is connected to yz and xy orbitals.

In Fig.2(a), we show LDA+DMFT momentum-resolved electronic spectra $A(\mathbf{k}, \omega)$ in the SDW phase. This quantity is probed by angle-resolved photoemission spectroscopy (ARPES). Figs.2(b) and (c) compare the Fermi surface of the PM and SDW states, displayed in the PM Brillouin zone.

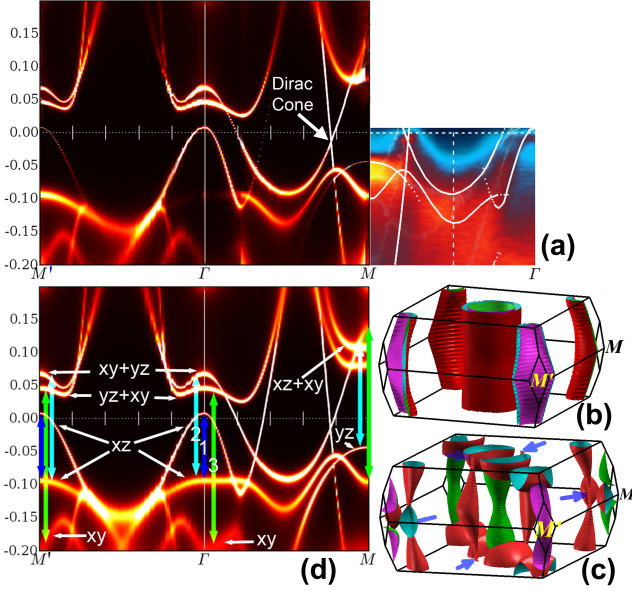


FIG. 2: ARPES and Fermi surface of BaFe_2As_2 . (a) $A(\mathbf{k}, \omega)$ in the Γ plane in the path $M' \rightarrow \Gamma \rightarrow M \rightarrow \Gamma$ of the SDW state. (See the locations of M and M' points in panel (b)). In the path $M \rightarrow \Gamma$ we overlaid ARPES data from Ref.[6]. (b) Fermi surface in the PM state. (c) Fermi surface in the SDW state, plotted in the PM Brillouin zone. Blue arrows mark the position of the Dirac cones. Note that the reciprocal vectors in the order state are $(1/2, -1/2, 0)$ in the direction of the ferromagnetic ordering, and $(1/2, 1/2, 1/2)$ in the direction of the antiferromagnetic ordering, hence points Γ and M' are equivalent, while points Γ and M are not. (d) $A(\mathbf{k}, \omega)$ in the SDW state with shadow bands plotted by equal intensity for clarity. Arrows mark the three types of optical transitions which give rise to the three peaks in the optical conductivity.

In the PM state, the topology of the Fermi surface is very similar to LDA predictions¹⁷ with three cylinders centered at Γ point and two at M point. In the SDW phase, the Fermi surface of the LSDA calculation (not

shown) and LDA+DMFT is very different. The magnetic order reconstructs the Fermi surface into smaller more three dimensional pockets. Out of three cylinders centered at Γ point, one remains in the SDW phase. This cylinder does not intersect the Γ plane within LSDA (not shown), but has been clearly identified in experiment. The other cylinders reconstruct into more three dimensional pockets.

In the SDW state, there are two inequivalent directions between Γ and M , here named M and M' , pointing along the antiferromagnetic and ferromagnetic direction of the Fe-Fe bonds, respectively. (see Fig. 2(b)). Graphene-like Dirac points were recently identified by ARPES along the antiferromagnetic direction⁶. Fig.2(a) shows that a crossing of two bands occurs very near the Fermi level between Γ and M , at 3/4 of the way, marked by a white arrow. The crossing is below the Fermi level, hence the pocket is electron like. In Fig. 2(c) we mark the same tiny pocket by blue arrows, to show that it has indeed a shape of a Dirac cone. There are two such symmetry related Dirac cones in the Γ plane and two in the Z plane. Notice that these cones appear only in the path between Γ to M (antiferromagnetic direction) and not in the Γ to M' .

In the most right-hand part of Fig. 2(a), we overlay our results with ARPES measurements of Richard *et al.*⁶, to emphasize common features. The overall position of the bands is in very good agreement without any need of shift of the Fermi level or renormalization of the bandwidth, in contrast to common need for shifts and renormalization when comparing DFT-derived bands with ARPES.

The LDA+DMFT Fermi surface also has good agreement with the ARPES measurement in the Z plane by Shimojima *et al.*¹⁸. In particular, the red electron pockets centered at Z , which have a two fold symmetry and mostly xz character, were identified in Ref.18.

In Fig. 2(d) we replot the momentum resolved electronic spectra $A(\mathbf{k}, \omega)$ without the SDW coherence factors, to enhance the shadow bands. The arrows in this graph connect the features in the electronic structure with the peaks in the optical conductivity. We mark three types of vertical transitions corresponding to the three peaks in Fig. 1. The first shoulder comes primarily from transitions within the xz orbital, namely between the flat band around -0.1 eV and the hole pocket at Γ and M . These transitions are between a shadow band and a non-shadow band, hence they appear only in the SDW phase. The second peak in optics, marked by cyan arrow, comes primarily from transitions between the xz and xy orbitals, with some transitions between non-shadow bands only, visible also in the PM state, and some additional transitions between a shadow and non-shadow band. Finally, the third peak comes mostly from transitions between the xy and yz orbitals, and mostly from transitions between a shadow to non-shadow band.

In correlated materials new physics, such as superconductivity, spin and orbital polarization, emerge from the competition between Coulomb interaction and kinetic en-

ergy.

A unique physical characteristics of iron arsenic materials is that the kinetic energy loss in the SDW phase is compensated by a gain in Hund's rule coupling energy. Comparison of the SDW and PM histograms, describing the probability of different iron configuration in the solid, shows that in the SDW state the high spin states become more probable. This results in an overall gain of the Hund's rule coupling energy of about 500 K per Fe. Overall kinetic energy is lost in the SDW state for about 300 K per Fe, resulting in a net energy gain of about 200 K per Fe. This is different from classical SDW transition where kinetic energy is compensated by the reduction of the Hubbard correlations.

The competition between kinetic and correlation energy takes different forms at different energy scales, and results in an unusual energy dependence of the spin and orbital polarization. Spin polarization affects most strongly the electrons far below the Fermi level. For example, the exchange splitting - as determined from the frequency dependent potential (self-energy) at high frequency - is three times larger than at zero frequency. This high frequency regime, is governed by the strong Hund's rule coupling on iron atom, enhancing magnetic moment.

At low energies, in the SDW state, well defined quasiparticles form, and the residual Hund's rule coupling between these quasiparticles is weak. To minimize the kinetic energy loss in the SDW phase, the quasiparticles propagate mainly along the antiferromagnetic x direction, the direction which is not blocked by the Pauli exclusion principle. This generates strong orbital polarization, but only at low energy, where the quasiparticles are well formed, and the effective Hund's rule coupling is weakest. On the contrary, the overall orbital polarization is weak.

Our finding that spin polarization is larger at high energy while the orbital polarization is most pronounced

at low energies leads to definite predictions for the anisotropy of the optical conductivity and can be tested also by STM.

Energy dependent polarizations and the enhancement of coherence of the low energy quasiparticles in the SDW phase, can only be described by frequency dependent potentials and Weiss fields, as is done in DMFT. This explains the failure of static mean field theories such as LDA to capture both the correct moment, which lives at high energies, and the low energy spectra. In a renormalization group picture of this material, one observes a different strength of the Hund's rule coupling at different energy scales. At high energy, Hund's rule coupling is very strong, while it fades away at low energy, but gives an imprint on the massive and anisotropic low energy quasiparticles. This is central for a proper description of the magnetic phase, and is likely to be important for the mechanism of the unconventional superconductivity in these materials.

METHOD

To show that the origin of the anisotropy is electronic rather than structural, we use the experimental lattice constants and internal coordinates of the paramagnetic phase⁷. We use the continuous time quantum Monte Carlo as the impurity solver and charge self-consistent version of LDA+DMFT, described in detail in Ref.19. We use *ab initio* determined Coulomb interaction strength $U = 5.0$ eV and $J = 0.7$ eV¹², and temperature $T = 72.5$ K. To explore the sensitivity of the magnetic moment to the strength of the Coulomb interaction, we performed calculations for other values of U and J around the *ab initio* values. We found that the size of the magnetic moment can be well parameterized by the simple formula $m = (0.4U + 7.2J - 6.1\text{eV})\mu_B/\text{eV}$. Hence, magnetization is most sensitive to the value of the Hund's coupling J , rather than U .

-
- ¹ Takabayashi, Y. *et al.* The disorder-free non-BCS superconductor Cs3C60 emerges from an antiferromagnetic insulator parent state. *Science* **323**, 1585 (2009).
 - ² Park, T. *et al.* Hidden magnetism and quantum criticality in the heavy fermion superconductor CeRhIn5. *Nature* **440**, 65 (2006).
 - ³ Huang, Q. *et al.* Neutron-diffraction measurements of magnetic order and a structural transition in the parent BaFe2As2 compound of FeAs-based high-temperature superconductors. *Phys. Rev. Lett.* **101**, 257003 (2008).
 - ⁴ Chu, J.-H. *et al.* Evidence for an electron nematic phase transition in underdoped iron pnictide superconductors. arXiv:1002.3364.
 - ⁵ Chuang, T.-M., *et al.* Nematic electronic structure in the "parent" state of the iron-based superconductor Ca(Fe1-xCo_x)2As2. *Science* **327**, 181 (2010).
 - ⁶ Richard, P. *et al.* Observation of Dirac cone electronic dispersion in BaFe2As2. *Phys. Rev. Lett.* **104**, 137001 (2010).
 - ⁷ Rotter, M. *et al.* Spin-density-wave anomaly at 140 K in

- the ternary iron arsenide BaFe2As2. *Phys. Rev. B* **78**, 020503(R) (2008).
- ⁸ Kotliar, G. *et al.* Electronic structure calculations with dynamical mean-field theory. *Rev. Mod. Phys.* **78**, 865 (2006).
- ⁹ Yin, Z. P. & Pickett, W. E. Antiphase magnetic boundaries in iron-based superconductors: a first-principles density-functional theory study. *Phys. Rev. B* **80**, 144522 (2009).
- ¹⁰ Hu, W. Z. *et al.* Origin of the spin density wave instability in AFe2As2 (A=Ba,Sr) as revealed by optical spectroscopy. *Phys. Rev. Lett.* **101**, 257005. (2008).
- ¹¹ Nakajima, M. *et al.* Evolution of the optical spectrum with doping in Ba(Fe1-xCo_x)2As2. *Phys. Rev. B* **81**, 104528 (2010).
- ¹² Kutepov, A., Haule, K., Savrasov, S. Y. & Kotliar, G. Self consistent GW determination of the interaction strength: application to the iron arsenide superconductors. arXiv:1005.0885.
- ¹³ Chen, Z. G., Yuan, R. H., Dong, T. & Wang, N. L. Optical spectroscopy of single-crystalline LaFeAsO. *Phys. Rev. B*

- 81**, 100502(R) (2010).
- ¹⁴ Qazilbash, M. M. *et al.* Mott transition in VO₂ revealed by infrared spectroscopy and nano-imaging. *Science* **318**, 1750 (2007).
 - ¹⁵ Yin, Z. P. *et al.* Electron-hole symmetry and magnetic coupling in antiferromagnetic LaFeAsO. *Phys. Rev. Lett.* **101**, 047001 (2008).
 - ¹⁶ Singh, R. R. P. Exchange constants and neutron spectra of iron pnictide materials. Arxiv:0903.4408.
 - ¹⁷ Singh, D. J. & Du, M.-H. Density functional study of LaFeAsO_{1-x}F_x: a low carrier density superconductor near itinerant magnetism. *Phys. Rev. Lett.* **100**, 237003 (2008).
 - ¹⁸ Shimojima, T. *et al.* Orbital-dependent modifications of electronic structure across the magnetostructural transition in BaFe₂As₂. *Phys. Rev. Lett.* **104**, 057002 (2010).
 - ¹⁹ Haule, K., Yee, C.-H. & Kim, K. Dynamical mean-field theory within the full-potential methods: electronic structure of Ce-115 materials. arXiv:0907.0195.

Supplementary Information is linked to the online version of the paper at www.nature.com/nature.

Acknowledgments ZPY is grateful to Chuck-Hou Yee for help at the initial stage of this project. We are grateful to D. Basov for fruitful discussions. ZPY and GK were supported by NSF DMR-0906943, KH was supported by NSF DMR-0746395 and Alfred P. Sloan foundation.

Author Information: Correspondence and requests for materials should be addressed to ZPY at yinzping@physics.rutgers.edu.

Magnetism and Charge Dynamics in Iron Pnictides

Supplementary Information

Z. P. Yin, K. Haule and G. Kotliar

Department of Physics and Astronomy, Rutgers University, Piscataway, NJ 08854, United States.

The two types of polarization, spin and orbital, are dominant at different energy scales. Spin polarization is stronger at higher energy (far below the Fermi level) while orbital polarization is strong at low energy (close to the Fermi level).

To demonstrate that the spin polarization is stronger at high energy, we plot in Fig. 3 the exchange splitting of iron $3d$ orbitals, defined by

$$\Sigma_{1,\uparrow}(\omega) - \Sigma_{1,\downarrow}(\omega).$$

Here $\Sigma(\omega)$ is the frequency dependent potential (self-energy), which is added to the one particle Hamiltonian, to produce the many body spectra. The high frequency limit of the exchange splitting is on average three times of its zero frequency value. Hence, the magnetic moment comes mainly from the high energy region, where the exchange splitting is large.

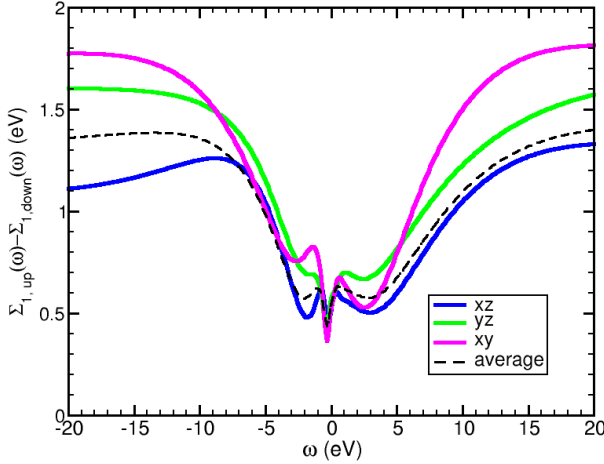


FIG. 3: Spin polarization of the frequency dependent self energy (real part) $\Sigma_{1,\uparrow}(\omega) - \Sigma_{1,\downarrow}(\omega)$ of the Fe $3d_{xz}$, $3d_{yz}$, $3d_{xy}$ orbitals, and the average over all five $3d$ orbitals in the SDW state of BaFe_2As_2 calculated by LDA+DMFT.

At energies within the SDW gap, the kinetic energy is dominant. To minimize the kinetic energy in the magnetically ordered state, electrons create a highway in the direction in which spins are antiferromagnetically ordered, while they remain slow in the ferromagnetic direction due to Pauli blocking. This gives rise to strong orbital polarization of the iron $3d$ orbitals at energies close to the Fermi level.

The orbital polarization is related to the frequency dependent Weiss field $\Delta(\omega)$, which describes the hybridization of the iron atom with the rest of the system. In Fig. 4 we plot the difference of the hybridization between the xz and yz orbital, i.e., $\Delta_{xz}(\omega) - \Delta_{yz}(\omega)$. In the paramagnetic state, the xz and yz hybridization are equal due to the tetragonal crystal structure, but they become different in the SDW state. As shown in Fig. 4 the orbital polarization acquires finite value only in the region of dominantly coherent spectra (within 1.5 eV from the Fermi level), and gets strongly enhanced within the SDW gap, where the quasiparticles are well defined.

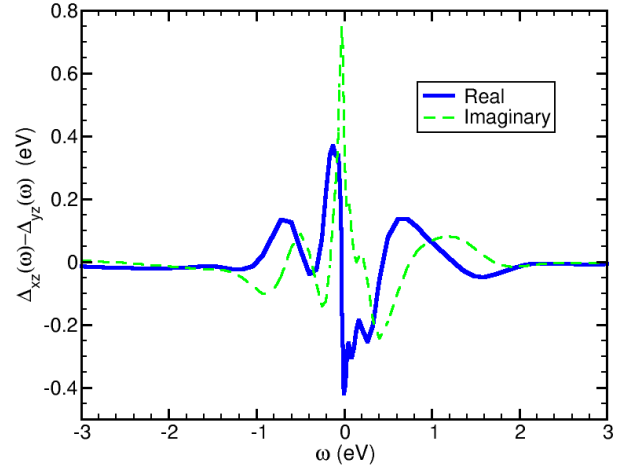


FIG. 4: Orbital polarization of the frequency dependent hybridization $\Delta_{xz}(\omega) - \Delta_{yz}(\omega)$ of the Fe $3d_{xz}$ and $3d_{yz}$ orbitals summing over both spin channels in the SDW state of BaFe_2As_2 calculated by LDA+DMFT.